Comparative study on the real-time monitoring of a fluid bed drying process of extruded granules using near-infrared spectroscopy and audible acoustic emission

Comparative study on the real-time monitoring of a fluid bed drying process of extruded granules using near-infrared spectroscopy and audible acoustic emission

Hisayoshi Aoki,[1)] Yusuke Hattori,[1)] Tetsuo Sasaki,[2,3)+] Makoto Otsuka[1,2)*]

[1)]Faculty of Pharmacy, Musashino University, 1-1-20 Shinmachi, Nishi-Tokyo, 202-8585, Japan
[2)]Research Institute of Electronics, Shizuoka University, 3-5-1 Johoku, Naka-ku, Hamamatsu, 432-8011, Japan
[3)]Graduate School of Medical Photonics, Shizuoka University, 3-5-1 Johoku, Naka-ku, Hamamatsu, 432-8011, Japan

[*]Corresponding author:
Makoto Otsuka, Ph.D.
E-mail: ohtsuka.makoto@shizuoka.ac.jp
Research Institute of Electronics,
Shizuoka University,
3-5-1 Johoku, Naka-ku, Hamamatsu, 432-8011, Japan
Phone: 053-478-3264

[+]Co-corresponding author:
Tetsuo Sasaki, Ph. D.
E-mail: sasaki.tetsuo@shizuoka.ac.jp
Graduate School of Medical Photonics, Shizuoka University,
Shizuoka University,
3-5-1 Johoku, Naka-ku, Hamamatsu, 432-8011, Japan

Abstract

The process of fluidized bed drying of granules was comparatively evaluated by on-line real-time measurements of granule moisture content (MC) using near-infrared spectroscopy (NIR) and audible acoustic emission (AAE). The extruded granules were prepared by kneading a powder blend containing lactose, starch, crystalline cellulose, and riboflavin, with water. The MC of the granules (while they were dried at 35 °C in a fluidized bed dryer) was monitored simultaneously with NIR and AAE. The prediction accuracy of the NIR and AAE using partial least squares (PLS) was verified by measuring MC of the granules. The best calibration models following NIR and AAE evaluations consisted of five latent variables with correlation coefficients of 1.000 and 0.998 and root mean square error of 0.259 and 0.615, respectively. As a result of external verification, the accuracy of MC analysis by AAE was slightly lower than that of NIR; however, it was still applicable in practice. Furthermore, the end point of fluidized bed drying process was automatically determined using the PLS discriminant analysis. From the above results, it can be concluded that the AAE-mediated granule drying process can be monitored with sufficient accuracy (compared with NIR).

Keywords: process analytical technology; calibration model robustness; fluid-bed drying; near-infrared spectroscopy; audible acoustic emission; partial least squares regression; granule drying

Introduction

Granules are prepared as aggregates with necessary functions for the desired purpose by devising the type and operating conditions of the granulator and dryer, the nature of the formulation additives, and the composition of the kneading fluid. Granule properties critical for the production of pharmaceutical dosage forms, such as particle size distribution, granule strength, fluidity, and moisture content (MC), have a significant impact on the critical quality attributes of the final products or dosage forms. To improve on product quality, process analytical technology (PAT) initiatives based on good manufacturing practices for medicines were proposed by the US Food and Drug Administration and the International Harmony Council [US Food and Drug Administration, 2009; US Food and Drug Administration, 2015]. The guidelines recommend that pharmaceutical quality assurance be achieved by employing a manufacturing process involving a design space where critical quality parameters are measured and controlled in real time using PAT tools [Yu, 2008; De Beer et al., 2011; Matero et al., 2013]. However, executing the manufacturing process in conjunction with real-time monitoring has been reported to be a challenge because of time and cost implications associated with the use of official Pharmacopeial analysis methods for the characterization of randomly extracted samples following the use of a conventional manufacturing process. Therefore, a combination method of near-infrared (NIR) spectroscopy and multivariate analysis [Martens & Naes, 1989] was introduced to the pharmaceutical industry as a monitoring technique for a manufacturing process, because this non-destructive analytical method could rapidly provide results with high accuracy based on a minimal amount of sample. NIR results provide information on the uniformity of the active ingredient in tablets [Blanco et al., 2000; Bodson et al., 2007; Alvarenga et al., 2008; Zidan et al., 2008], drug stability [Drennen & Lodder, 1990], powder particle size [Frake et al., 1998], tablet mechanical strength [Otsuka et al., 2006; Blanco et al., 2006], and dissolution rate [Donoso & Ghaly, 2004; Freitas et al., 2005; Gendre et al., 2011]. However, it has the disadvantage of being too costly to install because various NIR spectrometers will be required in various process steps on the factory production line.

In contrast, the acoustic emission (AE) method was developed to detect vital information based on process sound during manufacture. Similar to NIR spectroscopy, AE has the advantage of being a non-invasive technique in real time [Matero et al., 2013]. AE analytical methods applied in manufacturing process control can be divided into two types based on the frequency range of the applied sensors, viz. those that use the ultrasonic region (20,000 Hz or higher) and those that use the audible region (approximately 20–20,000 Hz). When using an ultrasonic AE sensor, it can easily be attached in close proximity to an instrument of container used in the production process to detect sound. Several research examples, such as particle size measurement [Leach et al., 1978; Leach & Rubin, 1978],

mixing [Tilly et al., 1988], agitation granulation [Whitaker et al., 2000], roller compression [Hakanen & Laine, 1995; Salonen et al., 1997], tablet compression [Waring et al., 1987; Tanaka et al., 2018], and tablet coating processes [Yoshida et al., 2001] have reported the application of the aforementioned technique. On the contrary, the use of audible AE (AAE) sensors involves detection of AAE propagating in the environment without physical contact [Briens et al., 2007; Bass et al., 2008; Daniher et al., 2008; de Martín et al., 2010]. As an online non-invasive PAT approach for predicting the characteristics of a pharmaceutical manufacturing control process, the AAE method with multivariate analysis was shown to be effective in monitoring the drying process in a fluidized bed dryer as well as the change in particle size distribution during agitation in granulation [Halstensen & Esbensen, 2000; Hansuld et al., 2009; Esbensen & Geladi, 2010; Li et al., 2011; Ihunegbo et al., 2013]. In our previous study [Aoki et al., 2014], we used the AAE method to monitor sound during the fluidized bed drying of extruded granules and analyzed the technique using a multivariate method, with subsequent establishment of a partial least square regression (PLS) calibration model with sufficient accuracy and robustness to measure the MC in the granules. In addition, we analyzed the regression vector of the calibration model to clarify, on a scientific basis, the mechanism of sound production during the drying process. To compare and evaluate the accuracy of the AE method as a PAT tool, Tok et al. [2008] simultaneously applied and compared three analytical techniques, viz. focused beam reflectance measurement, NIR, and AE. The fluidized bed granulation process could be measured semi-quantitatively using the three methods, and the mechanism of the granulation process was qualitatively elucidated. However, the quantitative accuracy of each method has not been reported, and a scientific difference is yet to be elucidated.

Consequently, in this study, dynamic change in the MC of pharmaceutical granules undergoing a fluidized bed drying process was simultaneously measured using the AAE and NIR methods by chemometrics, and the measurement accuracy and characteristics of the analytical methods were compared and interpreted. Furthermore, a partial least square-discriminant analysis (PLS-DA) [Martens & Naes, 1989; Peerapattana et al., 2013; Fordellone, et al., 2018; Mazivila, et al., 2015] was introduced to determine the MC of the granules and the end point (EP) of the drying process in real time.

Materials and methods

Materials

The active pharmaceutical ingredient (API), riboflavin (Wako Pure Chemical Industries, Ltd., Osaka, Japan), lactose monohydrate (Pharmatose® 200M, DMV, Veghel, Netherlands), a filler, potato starch (Kosakai Pharmaceutical Co., Ltd., Tokyo, Japan), a disintegrating agent, as well as microcrystalline cellulose (CEOLUS® PH-102, Asahi Kasei

Co., Ltd., Tokyo, Japan), hydroxypropylcellulose (HPC-L®, Nippon Soda Co. Ltd., Tokyo, Japan), and segregation preventive agents, were purchased from the local market.

Preparation of granules

Three hundred grams of powder blend consisting of API (3.0 g), lactose (200.0 g), potato starch (60.0 g), microcrystalline cellulose (27.0 g), and HPC-L® (10.0 g) was obtained by hand mixing in a polyethylene bag for 3 min. A wet mass was obtained by adding 100 mL of purified water in a mortar while kneading the mixture using a pestle. Next, wet extruded-granules were prepared using an extrusion granulator (KAR-130, Tsutsui Scientific Instruments Co., Ltd., Tokyo, Japan) equipped with a screen having a 1 mm diameter mesh. The granules were dried using a glass chamber fluidized bed dryer (SP-15, diameter 160 mm, volume 6.0 L, Okada Seiko Co., Ltd., Tokyo, Japan) equipped with a NIR spectrometer and a digital microphone as we reported in our previous study [Aoki et al., 2014]. The dryer was operated at an air inlet temperature of 35 °C for 20 min and an agitation speed of 180 rpm. Diffused reflectance NIR spectra and audible acoustic sound of the wet extruded granules were simultaneously measured during drying in the fluidized bed dryer, and 3 g of granular samples were collected from the sampling port of the dryer at regular intervals (every 2 min) during the process. NIR light was focused 3 cm from the edge of the chamber to the center, and the granule properties were measured during the drying process. The drying procedures were repeated three times (batches 1, 2, and 3) as calibration data sets and repeated once as a validation data set (batch V).

Measurement of granule MC

The weight loss of the granule samples collected during the drying process was weighed after storing 1 g of the sample at 70 °C for 24 h.

Evaluation of granule size distribution

The particle size of the granular samples after drying at 70 °C for 24 h was measured by the analytical serving method [Japanese Pharmacopeia 17] as follows: 10 g of the sample granules were placed on top of five sieve screens (355, 500, 850, 1180, and 1400 μm, Testing Sieve, Tokyo Screen Co., Ltd., Tokyo, Japan), and sieved manually. The weight of the sieved powder fractions was then measured using an electric microbalance. The particle size after drying was measured by a sieving method. Sample granules (10 g) were placed on top of five sieve screens (355, 500, 850, 1180, and 1400 μm, Testing Sieve, Tokyo Screen Co., Ltd.) and sieved manually according to the classification method. Then, the weight of the sifted powder fraction was measured using an electric microbalance.

Spectroscopic analysis by NIR

The NIR spectra of the fluidized bed drying process were obtained using a diffuse reflectance NIR spectrometer (MATRIX-F duplex, Bruker Optics, Ettlingen, Germany). The spectra were generated every 15 s for 20 min, and the measurement conditions were as follows: scan time: 16; resolution: 8 cm^{-1}; spectral range: 12000–4000 cm^{-1}.

Acoustic sound measurements

A digital voice recorder (RR-XS350, Panasonic Corporation, Tokyo, Japan) was set at 0.5 cm from the bottom wall of the chamber of the fluidized bed dryer, and the sounds emitted during the drying process were recorded as waveforms at a sampling rate of 44.1 kHz. The recorded sound signals at every 15 s for 20 min were transformed into frequency spectra using the fast Fourier transformation (FT) function of a computer software (Audacity® 2.0.5) [Audacity®, 2011]. The AAE frequency spectra for the semi-external validation data were transformed from the raw signals at every 60 s of every group 1, 2, and 3. In contrast, the spectra for the external validation data were transformed from the raw signals at every 60 s of group 8. The FT-AAE spectra included a window size of 4096 following the use of the Blackman-Harris window transformation, which involved a frequency range of 0–22 kHz. The frequency spectra were converted from amplitude to sound pressure level LP according to the following expression [Onosokki technical report].

$$L_P = 10log_{10}\frac{P^2}{{P_0}^2} , \quad (1)$$

where P is the actual sound pressure and P_0 is the reference sound pressure of 20 μPa in air. The actual sound pressure is related to the electromotive force E described in the following equation,

$$E = S + 10log_{10}P^2 , \quad (2)$$

$$P = 10^{\frac{E-S}{20}} , \quad (3)$$

where S is the sensitivity of the microphone. Substituting Eq. (3) to Eq. (1), the following equation can be derived,

$$L_P = E - S + 94 . \quad (4)$$

Multivariate analysis

The calibration models to predict the MC of the granule samples (the dependent variable) were obtained based on a total of 33 NIR spectra or 33 AAE spectra at predetermined sampling times in three repeated drying processes (batches 1, 2, and 3). The NIR and AAE spectra were corrected with various functions, including smoothing, area normalization, secondary derivative, multiplicative scatter correction, and standard normal variate [Aoki et al., 2014]. The best calibration models to predict the MC of the samples were determined based

on corrected NIR and AAE spectra using the leave-one-out cross-validation method in a chemometrics software (PLS, Pirouette® 4.5, Infometrix Inc. US).

The original descriptions of multivariate PLS [Martens and Naes, 1989] are as follows:

$$X = TP^T + E \qquad (5)$$

$$Y = UQ^T + F \qquad (6)$$

where X is an $n \times m$ matrix of predictors; Y is an $n \times p$ matrix of responses; T and U are $n \times m$ matrices of the X and Y scores, respectively; P and Q are $m \times l$ and $p \times l$ orthogonal loading matrices, respectively; and E and F are matrices of the error terms. The decompositions of X and Y are performed to maximize the covariance between T and U.

Multivariable analytical methods construct estimates of the linear regression between X and Y as follows:

$$Y = X\tilde{B} + \tilde{B}_0 \qquad (7)$$

where $\tilde{B}$ *and* $\tilde{B}_0$ are $n \times m$ matrices of related regression vector and errors, respectively.

The optimum number of latent variables (LV) was taken to be that leading to a minimum value in the prediction residual error sum of squares (*PRESS*) versus *PLS* component graph, which is defined as:

$$PRESS = \sum_{i=1}^{n} (\hat{y}_i - y_i)^2 \qquad (8)$$

where $\hat{y}_i$ and y_i correspond to the predicted and reference values, respectively. The goodness of the calibration model was assessed in terms of the standard error of prediction (*SEP,* also called as the root mean square error of prediction or *RMSEP*):

$$SEP = \sqrt{\frac{\sum_{i=1}^{n} (\hat{y}_i - y_i)^2}{n}} \qquad (9)$$

$$SEC = \sqrt{\frac{\sum_{i=1}^{n} (\hat{y}_i - y_i)^2}{n-k}} \qquad (10)$$

where n and k are the number of samples and LV, respectively, and *SEC* is the standard error of calibration.

Wet and dry granules with an MC of more and less than 0.5% w/w were classified as "class 1" and "class 0". The calibration models to predict class were constructed based on a total of 33 NIR spectra or 33 AAE spectra. The predicted class was determined using partial least squares discriminant analysis [Pirouette Multivariate Data, 2017; Brereton & Lloyd, 2014] (PLS-DA, chemometric software, Pirouette 4.5®, Infometrix Inc. US). Using the PLS-DA calibration model, the results showed that the granular fraction with the predicted class of more than 0.5 was classified as wet granules, and those with less than 0.5 were classified as dried, which was regarded as the best fit class prediction. An EP was defined as the drying time when the best fit class prediction changed twice in a row.

All data were examined based on three different measurement values and standard deviations (SD). Metric data were analyzed using one-way analysis of variance (ANOVA) at a significance level of 0.05.

Results

Simultaneous real-time evaluation of the granule MC during a fluid bed drying process using NIR spectroscopy and AAE

Figure 1 shows the results of the simultaneous measurements of NIR and AAE during the granule drying process of three batches. In the NIR spectra (Figure 1-a), as the drying process progressed, the absorption peak at 5160 cm^{-1} due to the combination tone (CT) between a stretch vibration (ST) and a deformation vibration (DEF) of the OH group attributable to free water [Osborne, 2006; Workman Weyer, 2012] was significantly decreased, and the peak at 6861 cm^{-1} due to the ST of the first overtone (OT) of the OH group attributable to free water [Osborne, 2006; Workman Weyer, 2012] also decreased. In contrast, the peak at 4660 cm^{-1} due to the CT between the ST and DEF of the OH group and that at 6495 cm^{-1} due to the ST of the 1st OT attributable to starch and cellulose [Osborne, 2006; Workman Weyer, 2012] increased.

From the changes observed in the AAE spectra of the samples during the drying process (Figure 1b), the granules had characteristic peaks at 161, 516, 3316, and 10831 Hz. The sound pressure level of the peaks at 161 and 516 Hz in the low frequency bands decreased to approximately 600 s (black dotted line) as the drying progressed, leading to a decrease in the MC. However, after 600 s of drying, the sound pressure increased slightly. Symmetrically, the sound pressure in the high frequency band of more than 4000 Hz, represented by the peaks at 3316 and 10831 Hz, increased as the MC decreased. To predict the MC of the granules, calibration models were constructed based on the various functions of pretreated NIR and AAE spectra using the cross-validation-leave-one-out method of the PLS technique. Figure 2 shows the best correlations between the predicted and actual MC levels of the granules following the use of the NIR and AAE methods. In addition, their chemometric parameters are summarized in Table 1. The best calibration model following NIR consisted of five LVs, and the PRESS Cal and SECV values were determined to be 1.81 and 0.329, respectively. The correlation plot showed a straight line with a slope of 0.999, a y-intercept of 0.0048, and a coefficient of determination (R^2) of 0.999. The best calibration model from the AAE technique consisted of five LVs, and the PRESS Cal and SECV values were 10.2 and 1.30, respectively. The correlation plot showed a straight line with a slope of 0.996, a y-intercept of 0.0273, and an R^2 value of 0.996. The lines due to 95% confidence intervals and 95% predictive intervals were represented in the correlation plots of NIR and AAE, respectively.

Figure 3 shows the regression vectors (RVs) of the best calibration models to predict the MC based on the NIR and AAE spectra. The RV of the calibration model based on the NIR

(Figure 3-a, dotted line) technique showed positive peaks at 7125, 5295, and 4956 cm^{-1} and a negative peak at 5160 cm^{-1}. The RV of the calibration model based on AAE (Figure 3-b, dotted line) showed a positive baseline shift at less than 200 Hz, a positive peak at 10551 Hz, and negative peaks at 3283 and 11197 Hz.

Figure 4 shows the verification results of the PLS calibration models based on the NIR and AAE spectra of the validation granule sample (batch V) during the fluid bed drying process. The predicted values of the MC in the granules by NIR (Figure 4-a) overlapped well with the measured values, and the 95% confidence interval of the predicted values was also quite narrow. The predicted MC s by AAE (Figure 4-b) also had slight gaps in the initial stage of drying; however, subsequent to this, the other values overlapped well with the measured values and were within the 95% confidence interval of the predicted values.

PLS-DA of the granule drying process in a fluidized bed dryer using NIR spectroscopy and AAE

To automatically determine the optimal EP of the granule drying process, calibration models to determine the drying class (0 or 1) of the granules were obtained based on NIR and AAE (Figure 1) by applying PLS-DA. The chemometric parameters of the best PLS-DA calibration models are listed in Table 2.

Figure 5 shows the results of the predicted class of the granules in relation to dryness using the best PLS-DA models based on individual NIR and AAE spectra. All the predicted classes of the wet granules evaluated based on NIR spectra by the PLS-DA model (Figure 5a) were more than 0.5, while those of the dry granules were less than 0.5. All predicted classes of the wet and dry granules based on AAE spectra were also more than 0.5, and less than 0.5, respectively (Figure 5a). The time profiles of the best-fit class prediction of the granules based on NIR and AAE during the drying process clearly showed the correct EP (Figure 5b).

To validate the obtained PLS-DA calibration models, external validation NIR and AAE data sets were evaluated using the best-fitted calibration models. Figure 6 shows the time profiles of the predicted class in relation to the dryness of the granules based on external NIR and AAE spectra as evaluated by PLS-DA calibration models. Following validation using the NIR method, the value of the predicted class for the granules decreased with increasing drying time, and the values were less than 0.5 at more than 600 s, with the groups of the symbols for the wet and dry granules being demarcated by the dotted line at 0.5 (Figure 6a). For the AAE validation procedure, the predicted dry class for the granules decreased with increasing time, and the values were less than 0.5 at more than 630 s, with the groups similarly being demarcated at the boundary of 0.5 (Figure 6b).

Figure 7 shows the best fit class-time profiles in relation to the dryness of the granules during the fluid bed drying process based on external NIR and AAE spectral data sets. The EP

of the drying process was also evaluated based on external NIR and AAE datasets. The EPs obtained by the NIR and AAE methods were 606 and 638 s, respectively.

Figure 3 shows the RVs of the PLS-DA calibration models to predict the class in relation to dryness of the granules based on NIR and AAE spectra. The RV of the model based on NIR (Figure 3-a, solid line) showed positive peaks at 4956 and 4470 cm^{-1} and negative peaks at 7329, 5345, and 5249 cm^{-1}. The RV of the model based on AAE (Figure 3-b, solid line) showed a positive peak at 495 Hz and many positive peaks between 1700–11000 Hz, a negative baseline shift at less than 200 Hz, and some negative peaks from 1000–1700 Hz.

Figure 8 shows the score plot of LV1 and LV2 of the PLS-DA calibration model based on the NIR spectra. The LV1 score increased monotonically during the drying process, while LV2 increased after the decrease, just before the EP. Figure 9 shows the score plot of LV1 and LV2 of the PLS-DA calibration model based on the AAE spectra.

The score plot of AAE also showed a similar trend to that observed using the NIR technique, with the LV1 score simply rising, while that of LV2 slightly increasing after the decrease and just before the EP.

Figure 10 shows the particle size distribution of granular samples at 0, 600, and 1200 s after drying. The particle size distribution of the granules was wider with increasing drying time, and the mode diameter of granule samples at 0, 600, and 1200 s was 1006, 487, and 448 μm, respectively.

Discussion

Comparative evaluation of granule MC during the fluidized bed drying process by PLS analysis using NIR spectroscopy and AAE

The MC of the granules was measured based on NIR adsorption peaks at 6861 and 5160 cm^{-1} due to free water (Figures 1a), as reported in previous studies [Osborne, 2006; Workman & Weyer, 2012]. The PLS calibration model to measure the MC of granules by the NIR method showed a good linear relationship between the predicted and measured values with relatively narrower confidence intervals and predictive intervals (Figure 2a and Table 1). This suggests that the NIR is a highly accurate and reproducible method. The RV of this model (Figure 3a) had several peaks at approximate values of 7000 and 5000 cm^{-1} due to the OH group. This result indicated that the calibration model using NIR was dependent on variability based on the reduction of free water. Additionally, because the RV of the calibration model was based on the specific chemical information analyzed by NIR due to OH in water, it was indicated that the model was not due to over-calculation of the noise signal dependence.

On the other hand, in the AAE measurements, the AAE peak intensity in the low frequency range of 10–6000 Hz decreased and those in the high frequency range above 1800 Hz increased as drying progressed (Figure 1b). The PLS calibration model of AAE showed a good linear relationship between the predicted and measured values with relatively wider

confidence interval and predictive interval (Figure 2b and Table 1). It was challenging to reproduce measurement in the plain fluid bed drying process by AAE. However, as shown here, the acoustic reproducibility could be improved by rotating the fluidized powder bed at 100 rpm using a stirring rod to generate the sound of granules. Therefore, the result suggested that the modified AAE method could accurately measure the MC in granules but at insufficient precision due to less reproducibility compared to the NIR method. The RV (Figure 3b) had a positive plateau peak between 10–6000 Hz in the low frequency range, and several negative peaks from 1800–11000 Hz in the high frequency range. The result of the PLS calibration model by AAE indicated that at the initial stage of the fluidized bed drying process, the moist granular mass produced low frequency sounds due to the rotation of the stirring bar. Subsequently, the low frequency sounds decreased depending on the progress of drying, while the high frequency sounds increased. Therefore, the RV of the AAE calibration model was based on the specific physical properties of the granules, thus concluding that this might not be due to over-calculation.

To validate the PLS calibration models based on NIR and AAE spectra of granule samples during the drying process, the MC in the external granule samples were simultaneously predicted by NIR and AAE methods (Figure 4). Both the predicted values of the MC in the granules by NIR and AAE (Figure 4) overlapped well with the measured values, and the 95% confidence interval of the predicted values was also sufficiently narrow. However, the 95% confidence intervals of the values predicted by AAE were slightly wider than those predicted by NIR, which might be practically acceptable values. SEC and PRESS for calibration (PRESS Cal) were related to the precision of the calibration model for predicting the MC in granules (Figure 4 and Table 1). The values of AAE were larger than those of NIR; however, the coefficient of determination for calibration (R^2 Cal) of AAE in relation to accuracy was almost the same as that of the NIR method. The results of validation by NIR and AAE showed that the predicted and measured values were in close agreement. These results confirmed that the best calibration models using NIR and AAE could accurately predict the MC of the granules.

Automatic evaluation of the end point of the granule drying process in a fluidized bed dryer by PLS-DA using NIR spectroscopy and AAE

To prepare an automated manufacturing process for pharmaceutical dosage forms, it is necessary to establish a management system to automatically evaluate the critical quality attributes of the formulations based on the obtained product characteristic information in all processes by using nondestructive and non-contact real-time monitoring. Therefore, in this study, to obtain information in order to rapidly advance to the subsequent process following the drying process in the fraction granule drying process, an automatic verification method was investigated to ensure that the dryness of the granule fraction was below a constant MC.

PLS-DA was applied to the NIR and AAE spectral datasets (Figure 1) of the granules from batches 1, 2, and 3, and the calibration models were prepared to identify whether the granule samples were dry (Class 0; MC was less than 0.5 %w/w) or wet (Class 1; MC was more than 0.5 %w/w). The PLS-DA analytical results based on the calibration data of NIR and AAE (Figure 5b) showed that dried granules could be automatically identified with good reproducibility by the NIR and AAE methods. Furthermore, in order to clarify the scientific evidence for the mechanism of identification of these calibration models, the relationship between the spectroscopic or acoustic elements of the models and the physicochemical elements of the drying process was examined.

LV was systematically added into the PLS-DA models based on NIR and AAE, and the SECV decreased until thresholds were established. Therefore, the best calibration models consisted of five LVs at the lowest SECV s (SECV =0.184 and 0.242) (Table 2). The chemometric parameters, such as SEC, PRESS Cal, and R^2 Cal, of the PLS-DA models to predict the class of dryness of the granules were not significantly different between NIR and AAE. However, SECV and PRESS Val of NIR were significantly lower than those of AAE, and the cumulative percent variable (CPV) and coefficient of determination based on cross-validation (R^2 Val) of NIR were significantly higher than those of AAE. In the cross-validation result (Figure 5a) of classes in relation to dryness of the granules by NIR and AAE, predicted classes of all wet granules were more than 0.5, and those of the dry granules were less than 0.5. The calibration data sets of NIR and AAE were correctly classified into classes using both analytical methods, respectively (Figure 5a). Therefore, the final evaluation of EPs (Figure 5b) based on the time profile of best-fit class prediction of the granules by NIR and AAE methods yielded accurate results.

To validate the PLS-DA calibration model, the external NIR dataset for validation was evaluated using an optimal calibration model (Figure 6a). The values of the prediction class in relation to dryness of granules decreased with increasing drying time, and the values decreased to less than 0.5 at 600 s or more. With the AAE validation process (Figure 6b), the values of the predicted class decreased with increasing drying time, and were less than 0.5 at more than 630 s. The PLS-DA results of the NIR and AAE methods indicated that both techniques could be clearly used to classify granules into wet and dry groups with a dotted separation line at 0.5.

The EP of the drying process was evaluated to be 606 s from the best-fit class prediction-time profile of the granules during the fluidized bed drying process based on external NIR datasets (Figure 7). Similarly, the EP of the drying process evaluated by AAE was 638 s, and the value could be evaluated as almost similar to that observed with the NIR method. The results of validation based on external NIR and AAE data indicated that the best PLS-DA calibration models were able to accurately assess the classification associated with granule drying.

Classification of granules with regards to dryness by PLS-DA using NIR spectroscopy and AAE

To elucidate the scientific reasoning behind the determination of granule classification based on dryness, the RVs of the PLS-DA calibration models were investigated. Using the NIR method, the RVs of the PLS and PLS-DA calibration models (dotted line and solid line in Figure 3-a, respectively) showed specific peaks due to free water at approximately 5000 cm^{-1} and 7300 cm^{-1}. Therefore, the result suggested that the calibration models by NIR reflected a decrease in the MC during the drying process. However, the RV pattern of PLS-DA was similar but not identical to that of PLS. Because the PLS model was used to quantitatively predict the amount of MC in the granules, the PLS-DA model was determined to be a qualitatively predicted class in relation to dryness (<0.5% w/w MC) of the granules.

With the AAE method, the RVs of the PLS and PLS-DA calibration models (dotted line and solid line in Figure 3-b, respectively) had similar patterns of a decrease in low frequency sounds and an increase in high frequency sounds. Nevertheless, they were upside down and the latter had a specific peak at 495 Hz. In addition, the RV of PLS-DA was somewhat different from that of PLS. Furthermore, to elucidate the molecular mechanism and sound generation mechanism of the granules in the fluid-bed drying process, molecular mechanism analysis was performed focusing on the kinetic changes of each latent variable obtained from multivariate analysis data from NIR and AAE. The LV1 and LV2 score plots of the PLS-DA calibration model based on the NIR spectra are depicted in Figure 8a. LV1 showed peaks at 7100 and 5220 cm^{-1} due to free water and the peak at 5100 cm^{-1} due to crystalline water [Osborne, 2006; Workman & Weyer, 2012] (Figure 8b). LV2 had a positive peak at 7100 cm^{-1} due to free water and a negative peak at 5180 cm^{-1} due to the bound water of carbohydrates as excipients [Osborne, 2006; Workman & Weyer, 2012] (Figure 8c). This score profile indicated that the LV1 score increased monotonically with decreasing total MC, while the LV2 score profile suggested that some of the free water transformed to bound water during drying.

In contrast, in the calibration model determined by AAE, LV1 (17.7%) showed negative peaks at low and mid frequency bands (around 100 and 1000 Hz, respectively) (with a specific positive peak at 495 Hz), and positive peaks for high frequency bands between 2000–6700 Hz (Figure 9b). While LV2 (47.9%) (Figure 9c) had positive peaks at low and mid frequency bands (with a specific positive peak at 495 Hz). Moreover, no specific peak at high band was observed. The result indicated that acoustic components in LV1 involved a decrease in low and mid frequency sounds and an increase in high frequency sounds generated during drying of the granules. Additionally, the LV1 score simply increased with decreasing MC, similar to the NIR results. However, LV2 involved only low frequency sounds at less than 3000 Hz, and it increased after 600 s drying time. This suggested that the granules at 600 and 1200 s were almost completely dry, but their sounds were slightly different from each other.

Although the measurement was done by analytical methods based on different mechanisms, both score plot results of NIR and AAE indicated similar phenomena during the drying process. Therefore, the granule dehydration in the fluid-bed dryer might be considered to follow a molecular mechanism as follows: Difference types of water exist in the powder formulation system, such as crystal water, bonding water, and surface adsorbed water of lactose monohydrate, crystalline cellulose, API, and starch. Many types of water in the formula powder are in equilibrium with a water vapor pressure depending on the chemical potential of each solid compound, as their vapor pressure level differ. Additionally, there were temperature and vapor pressure distribution patterns in the fluidized bed drying chamber between the surface and inside the granule surface and the upper and lower parts of the powder layers.

In the NIR score plot (Figure 8a), most of the water contained in the granules was free water represented by the LV1 and was dehydrated in the drying process. In contrast, some water represented as LV2 was a hydrogen bonded water or due to OH group, and hence, it might be resorbed due to strong hydrogen bonding of excipients in the drying process after the dehydrated.

While, in the AAE score plot (Figure 9a), LV1 score was simply increased with increasing drying time, LV2 score was decreased up to 600 s and then increased. A reduction in granule size has been shown in all drying processes (Figure 10). As the size of the physical granule was closely related to the vibration frequency, Eq. (11) shows a relation of the natural frequency between frequency and length of the subject [Hartog, 1985].

$$\nu = \frac{x}{2l}\sqrt{\frac{T}{\rho}} \qquad x=1, 2, 3, \ldots, \tag{11}$$

where ν is the frequency, T is the linear density, and l is the length.

Considering the changes in AAE during the granule drying process based on Eq. (11) in the AAE score plot (Figure 9a), the natural frequency in LV1 might be changed due to a significant reduction in granule length during the drying process up to 600 s with MC weight loss (Fig. 10). After more than 600 s, the natural frequency of LV2 might change due to a slight decrease in granule size due to the flow of granules without MC weight loss. Furthermore, MC in the granules could also affect the natural vibration through the changes in the length and linear density of the granules.

Moreover, the precision and accuracy of PLS-DA analysis (Table 2) by the NIR and AAE methods were compared with those of PLS. In the case of PLS analysis to quantitatively predict the MC in the granules, the NIR method was superior in precision (SEC and PRESS) and accuracy (R^2). Although the AAE method was slightly inferior in terms of precision, the statistical value for accuracy was almost similar to that of NIR. In contrast, in the PLS-DA method, both the NIR and AAE methods showed almost identical statistical values in terms of precision and accuracy. Because the EP was indirectly evaluated based on the classification parameters-time profiles of granules by the PLS-DA method (Figure 7), it might be postulated

that the NIR and AAE methods showed similar accuracy without any statistical difference ($P < 0.05$).

Conclusions

In this study, the usefulness of real-time monitoring with NIR and AAE analysis was evaluated to predict the MC of granules and the EP of a fluidized bed drying process. The calibration models for determining the MC of the granules were constructed using NIR and AAE with PLS. In addition, the EP was determined using PLS-DA calibration models based on NIR and AAE spectra. The AAE method was compared with the NIR method, and the findings showed AAE as a similarly useful technique to NIR for monitoring the drying process of granules. High-accuracy NIR is one of the most promising monitoring tools for PAT; however, the high initial cost of implementation remains a challenge. In this study, it was shown that the AAE method had almost the same EP evaluation ability as NIR in terms of accuracy. Therefore, if the AAE technology is further improved, it can be expected to serve as a simple and inexpensive measurement method for monitoring the granule drying process.

Acknowledgments

This research received partial financial support from the Research Institute of Electrics, Shizuoka University, and Research Center for Biomedical Engineering (2021-No. 2033).

Declaration of Interests

The authors have no direct conflicts of interest relevant to the contents of this manuscript.

References

Alvarenga L., Ferreira D., Altekruse D., Menezes J.C., Lochmann D., 2008. Tablet identification using near-infrared spectroscopy (NIRS) for pharmaceutical quality control, *J. Pharm. Biomed. Anal.*, 48(1), 62–69.

Aoki H., Hattori Y., Otsuka M., 2014. Real-time monitoring of the drying of extruded granules in a fluid-bed dryer using audible acoustic emission chemometrics, *RSC Adv.*, 4(92), 50558–50565.

Audacity® (Audacity 2.0.5, http://audacity.sourceforge.net), November 11 2011.

Bass H.E., Campanella A.J., Chambers J.P., Lindsay R.B., 2008. Sound absorption. AccessScience@McGraw-Hill. Accessed May 14, 2008, from http://www.accessscience.com.proxy2.lib.uwo.ca:2048, doi:10.1036/1097-8542.637300.

Blanco M., Alcalá M., González J.M., Torras E., 2006. A process analytical technology approach based on near infrared spectroscopy: Tablet hardness, content uniformity, and dissolution test measurements of intact tablets, *J. Pharm. Sci.*, 95(10), 2137–2144.

Blanco M., Eustaquio A., González J.M., Serrano D., 2000. Identification and quantitation assays for intact tablets of two related pharmaceutical preparations by reflectance near-infrared spectroscopy: validation of the procedure, *J. Pharm. Biomed. Anal.*, 22(1), 139–148.

Bodson C., Rozet E., Ziemons E., Evrard B., Hubert P., Delattre L., 2007. Validation of manufacturing process of diltiazem HCl tablets by NIR spectrophotometry (NIRS), *J. Pharm. Biomed. Anal.*, 45(2), 356–361.

Brereton R.G., Lloyd G.R., 2014. Partial least squares discriminant analysis: taking the magic away, *J. Chemom.*, 28(4), 213–225.

Briens L., Daniher D., Tallevi A., 2007. Monitoring high-shear granulation using sound and vibrationmeasurements, *Int. J. Pharm.*, 331(1), 54–60.

Daniher D., Briens L., Tallevi A., 2008. End-point detection in high-shear granulation using sound and vibration signal analysis, *Powder Technol.*, 181(2), 130–136.

De Beer T., Burggraeve A., Fonteyne M., Saerens L., Remon J.P., Vervaet C., 2011. Near infrared and Raman spectroscopy for the in-process monitoring of pharmaceutical production processes, *Int. J. Pharm.*, 417(1–2), 32–47.

de Martín L., Villa Briongos J., Aragón J.M., Palancar M.C., 2010. Can low frequency accelerometry replace pressure measurements for monitoring gas–solid fluidized beds?, *Chem. Eng. Sci.*, 65(13), 4055–4064.

Donoso M., Ghaly E.S., 2004. Prediction of drug dissolution from tablets using near-infrared diffuse reflectance spectroscopy as a nondestructive method, *Pharm. Dev. Technol.*, 9(3), 247–263.

Drennen J.K., Lodder R.A., 1990. Nondestructive near-infrared analysis of intact tablets for determination of degradation products, *J. Pharm. Sci.*, 79(7), 622–627.

Esbensen K.H., Geladi P., 2010. Principles of proper validation: use and abuse of re-sampling for validation, *J. Chemom.*, 24(3–4), 168–187.

Frake P., Gill I., Luscombe C.N., Rudd D.R., Waterhouse J., Jayasooriya U.A., 1998. Near-infrared mass median particle size determination of lactose monohydrate, evaluating several chemometric approaches, *Analyst*, 123(10), 2043–2046.

Fordellone, M., Bellincontro, A., & Mencarelli, F., 2018. Partial least squares discriminant analysis: A dimensionality reduction method to classify hyperspectral data. Statistica Applicata -, *Italian J. Applied Statistics,* 31(2), 181–199.

Freitas M.P., Sabadin A., Silva L.M., Giannotti F.M., do Couto D.A., Tonhi E., Medeiros R.S., Coco G.L., Russo V.F.T., Martins J.A., 2005. Prediction of drug dissolution profiles from tablets using NIR diffuse reflectance spectroscopy: a rapid and nondestructive method, *J. Pharm. Biomed. Anal.*, 39(1–2), 17–21.

Gendre C., Boiret M., Genty M., Chaminade P., Pean J.M., 2011. Real-time predictions of drug release and end point detection of a coating operation by in-line near infrared measurements, *Int. J. Pharm.*, 421(2), 237–243.

Hakanen A., Laine E., 1995. Acoustic characterization of a microcrystalline cellulose powder during and after its compression, *Drug Dev. Ind. Pharm.,* 21(13), 1573–1582.

Halstensen M., Esbensen K., 2000. New developments in acoustic chemometric prediction of particle size distribution-'The problem is the solution', *J. Chemom.*, 14(5–6), 463–481.

Hansuld E.M., Briens L., McCann J.A.B., Sayani A., 2009. Audible acoustics in high-shear wet granulation: application of frequency filtering, *Int. J. Pharm.*, 378(1–2), 37–44.

Den Hartog, J. P., 1985. *Mechanical vibrations*. Courier Corporation.

Ihunegbo F.N., Ratnayake C., Halstensen M., 2013. Acoustic chemometrics for on-line monitoring and end-point determination of fluidised bed drying, *Powder Technol.*, 247, 69–75.

Japanese Pharmacopeia 17, 3. 04. Particle size determination, 2. Method 2 Analytical serving method, February 23, 2022, chrome-extension://efaidnbmnnnibpcajpcglclefindmkaj/viewer.html?pdfurl=https%3A%2F%2Fwww.mhlw.go.jp%2Ffile%2F06-Seisakujouhou-11120000-Iyakushokuhinkyoku%2FJP17_REV_1.pdf&clen=105618970&chunk=true

Leach M.F., Rubin G.A., 1978. Size analysis of particles of irregular shape from their acoustic emissions, *Powder Technol.,* 21(2), 263–267.

Leach M.F., Rubin G.A., Williams J.C., 1978. Particle size distribution characterization from acoustic emissions, *Powder Technol.*, 19(2), 157–167.

Li Y., Grace J.R., Gopaluni R.B., Bi H., Lim C.J., Ellis N., 2011. Characterization of gas–solid fluidization: A comparative study of acoustic and pressure signals, *Powder Technol.*, 214(2), 200–210.

Martens H., Naes T., 1989, Multivariate calibration. New York: John Wiley & Sons.

Matero S., van Den Berg F.V., Poutiainen S., Rantanen J., Pajander J., 2013. review. Towards better process understanding: chemometrics and multivariate measurements in manufacturing of solid dosage forms, *J. Pharm. Sci.,* 102(5), 1385–1403.

Mazivila, S. J., de Santana, F. B., Mitsutake, H., Gontijo, L. C., Santos, D. Q., Neto, W. B., 2015. Discrimination of the type of biodiesel/diesel blend (B5) using mid-infrared spectroscopy and PLS-DA. *Fuel,* 142, 222–226.

Osborne B.G., Near-infrared spectroscopy in food analysis. Encyclopedia of analytical Chemistry: applications, Theory and instrumentation, 2006.

Otsuka M., Yamane I., 2006. Prediction of tablet hardness based on near infrared spectra of raw mixed powders by chemometrics, *J. Pharm. Sci.,* 95(7), 1425–1433.

Peerapattana J., Shinzawa H., Otsuka K., Hattori Y., Otsuka M., 2013. Partial least square discriminant analysis of mangosteen pericarp powder by near infrared spectroscopy, *J. Near Infrared Spec.,* 21, 195–202.

U.S. Food and Drug Administration Center for Drug Evaluation and Research home page, *'Process Anal. Technol. (Pat.) Initiat.'* Accessed August 12 2009, from http://www.fda.gov/AboutFDA/CentersOffices/OfficeofMedicalProductsandTobacco/CDER/ucm088828.htm.

Salonen J., Salmi K., Hakanen A., Laine E., Linsaari K., 1997. Monitoring the acoustic activity of a pharmaceutical powder during roller compaction, *Int. J. Pharm.,* 153, 257–261.

Onosokki technical report, Sound & Vibration Technologies - about the sensor and sound -, http://www.onosokki.co.jp/HP-WK/c_support/newreport/sound/soundsensor.pdf, (accessed December 2013).

Pirouette multivariate data, analysis software, version 4.5. 11807 North Creek Parkway S: Infometrix Inc., Suite B.-111, Bothell, WA98011, from http://www.infometrix.com/, March 18, 2017.

Tanaka R., Kojima K., Hattori Y., Ashizawa K., Otsuka M., 2018. Audible acoustic emission data analysis for active pharmaceutical ingredient concentration prediction during tableting processes, *Int. J. Pharm.,* 548(1), 721–727.

Tilly P.J., Porada S., Scruby C.B., Lidington S. Monitoring of mixing processes using acoustic emission. In: Harnby N, Benkreira H, Carpenter KJ, Mann R, editors. Fluid mixing III. Rugby, Warks: *Institution of Chemical Engineers,* 1988.

Tok A.T., Goh X., Ng W.K., Tan R.B., 2008. Monitoring granulation rate processes using three PAT tools in a pilot-scale fluidized bed, *AAPS PharmSciTech*, 9(4), 1083–1091.

US Food and Drug Administration, "International Conference on Harmonization of Technical Requirements for Registration of Pharmaceuticals for Human Use. Pharmaceutical, *Development*, Q8(R2). Accessed August 15 2015, from http://www.fda.gov/downloads/Drugs/GuidanceComplianceRegulatoryinformation/Guidances/ucm073507.pdf.

Waring M.J., Rubinstein M.H., Howard J.R., 1987. Acoustic-emission of pharmaceutical materials. The effect of compression speed, ejection, lubrication and tablet weight, *Int. J. Pharm.,* 40, 15–22.

Whitaker M., Baker G.R., Westrup J., Goulding P.A., Rudd D.R., Belchamber R.M., Collins M.P., 2000. Application of acoustic emission to the monitoring and end point determination of a high shear granulation process, *Int. J. Pharm.*, 205(1–2), 79–92.

Workman Jr J., Weyer L., 2012, Practical guide and spectral atlas for interpretive near-infrared spectroscopy. CRC Press Co., Ltd.

Yoshida T., Tanino T., Sumi Y., Nogami F., 2001, Coating and polishing methods, and the surface treatment apparatus to do by the methods, *Tokkai-Patent* 2001–252548 (P 2001–252548A).

Yu L.X., 2008. Pharmaceutical quality by design: Product and process development, understanding and control, *Pharm. Res.,* 25(4), 781–791.

Zidan A.S., Habib M.J., Khan M.A., 2008. Process analytical technology: Nondestructive evaluation of cyclosporine A and phospholipid solid dispersions by near infrared spectroscopy and imaging, *J. Pharm. Sci.,* 97(8), 3388–3399.

Figure Captions

Figure 1. Changes in NIR and AAE spectra of granules from three batches during the fluid bed drying process.

(a) NIR spectra; (b) AAE spectra; red solid line, initial spectrum; black solid line, final spectrum; black dotted line, spectrum at approximately 600 s; blue solid line, spectrum of pure water; ST, stretch vibration; OT, overtone; DEF, deformation vibration; CT, combination tone.

Figure 2. Relationships between predicted and actual MC of the granules by best fit PLS regression calibration model using NIR and AAE methods.

Open triangle, near-infrared method; closed circle, audible acoustic emission method; dotted line, 95% confidence interval; dash line, 95% predictive interval.

Figure 3. Regression vectors of calibration models to predict the MC or class in relation to dryness of granules during the fluid bed drying process.

(a) NIR method; (b) AAE method; solid line, PLS-DA; dotted line, PLS.

Figure 4. Verification of PLS calibration models based on NIR and AAE spectra of granules (batch V) during a fluid bed drying process.

Open triangle, predicted the MC by NIR method; closed circle, predicted the MC by AAE method; open circle, measured moisture content; dotted lines, 95% confidence limit.

Figure 5. Relationships between predicted and actual class in relation to dryness of the granules using the PLS-DA models based on individual NIR and AAE spectra.
(a) plots of predicted vs. actual class in relation to the dryness of the granules; (b) the drying time profiles of the best predicted class of the granules; actual class 1, wet granules (> 0.5% w/w MC); actual class 0, dry granules (< 0.5% w/w MC); open triangle, NIR method; closed circle, AAE method.

Figure 6. Time profiles of predicted class in relation to dryness of the granules based on external NIR and AAE spectra by PlS-DA calibration models as validation results.
(a) NIR method; (b) AAE method; open symbol, dry granules; closed symbol, wet granules.

Figure 7. Time profiles of the best fit class in relation to dryness of granules based on external NIR and AAE spectra by PLS-DA calibration models as validation results.
Triangle, NIR method; circle, audible AAE method; open symbol, dry granules; closed symbol, wet granules.

Figure 8. Score plot of LV1 and LV2 of PLS-DA calibration model based on NIR spectra.
(a) score plot of LV1 and LV2; (b) loading vector of LV1; (c) loading vector of LV2.

Figure 9. Score plot of LV1 and LV2 of PLS-DA calibration model based on AAE spectra.
(a) score plot of LV1 and LV2; (b) loading vector of LV1; (c) loading vector of LV2.

Table captions

Table 1. Chemometric parameters of partial least squares regression calibration models to predict the moisture content of granules by NIR and AAE methods.
LV: number of latent variables; CPV: cumulative percent variable; SECV: standard error of cross-validation; PRESS Val: prediction residual error sum of squares based on validation; PRESS Cal: prediction residual error sum of squares based on calibration; SEC: standard error of calibration; R^2 Val: coefficient of determination based on cross-validation; R^2 Cal: coefficient of determination for calibration.

Table 2. Chemometric parameters of PLS-DA calibration models to predict the class in relation to dryness of the granules by NIR and AAE methods.
LV: number of latent variables; CPV: cumulative percent variable; SECV: standard error of cross-validation; PRESS Val: prediction residual error sum of squares based on validation; PRESS Cal: prediction residual error sum of squares based on calibration; SEC: standard

error of calibration; R^2 Val: coefficient of determination based on cross-validation; R^2 Cal: coefficient of determination for calibration.

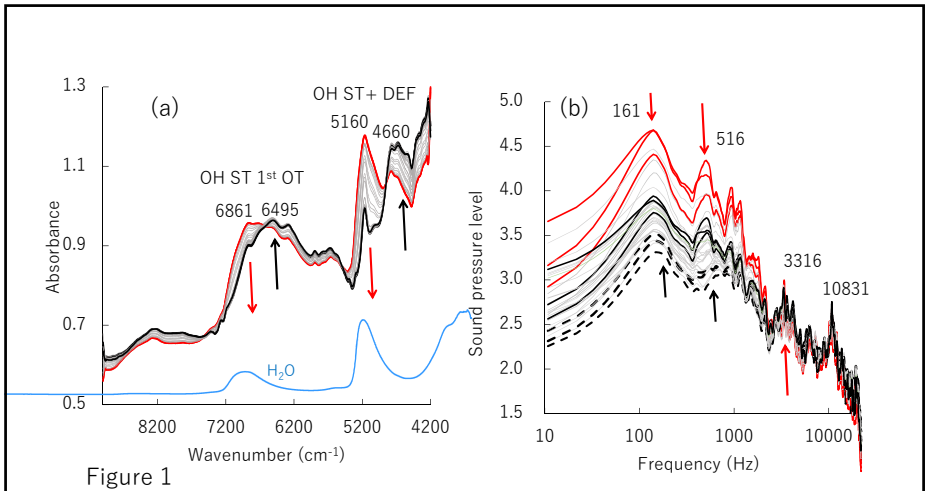

Figure 1

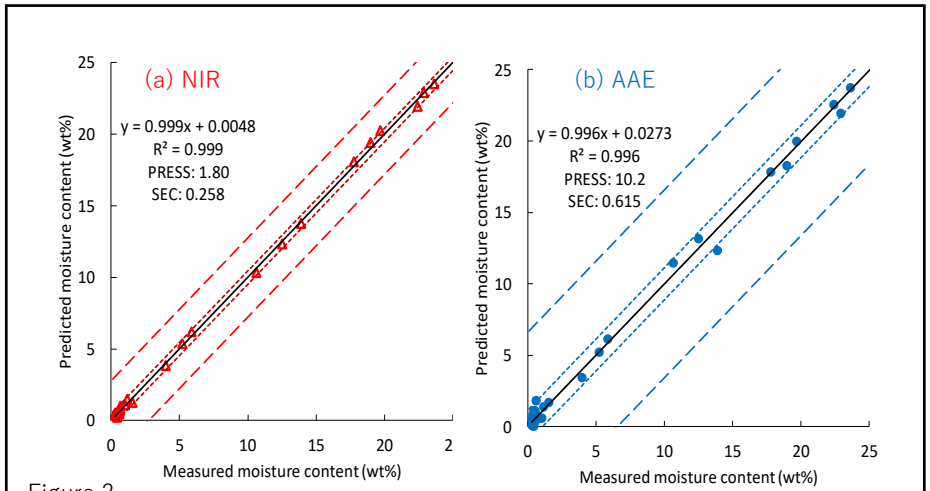

Figure 2

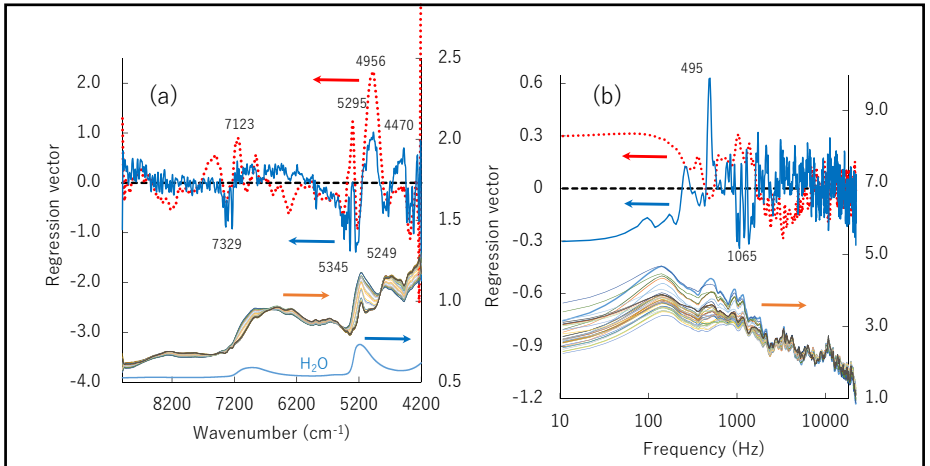

Figure 3

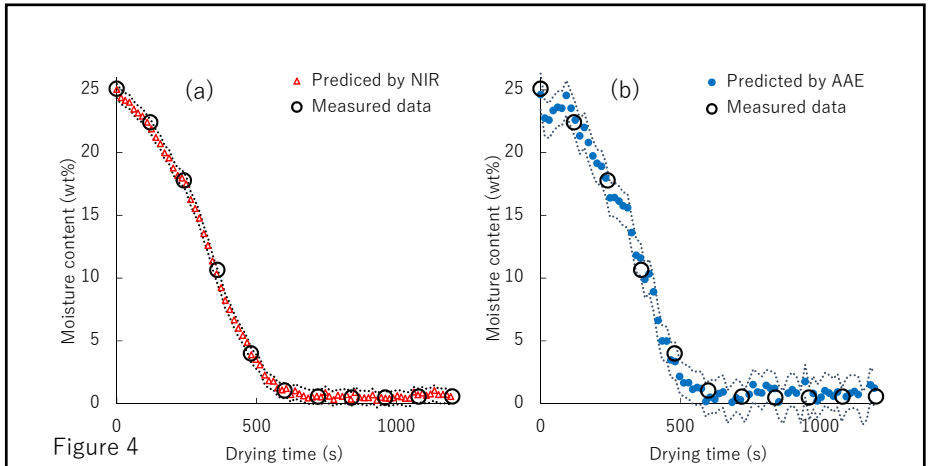

Figure 4

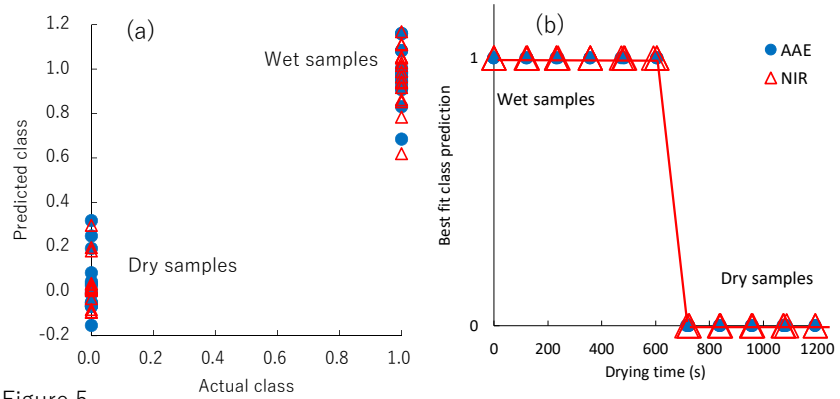

Figure 5

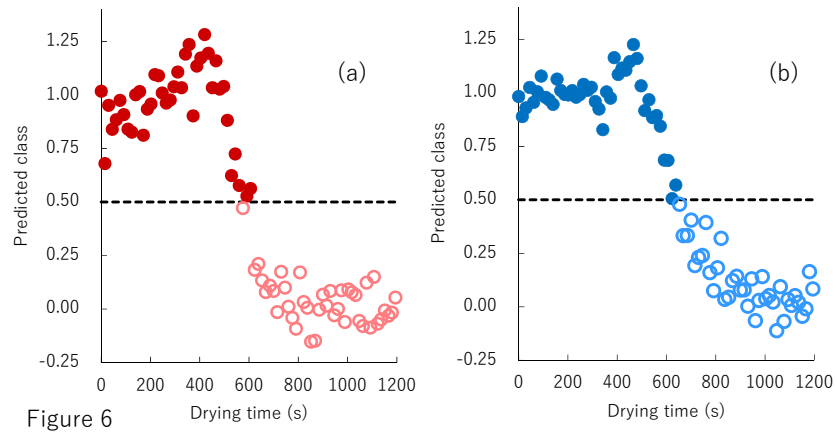

Figure 6

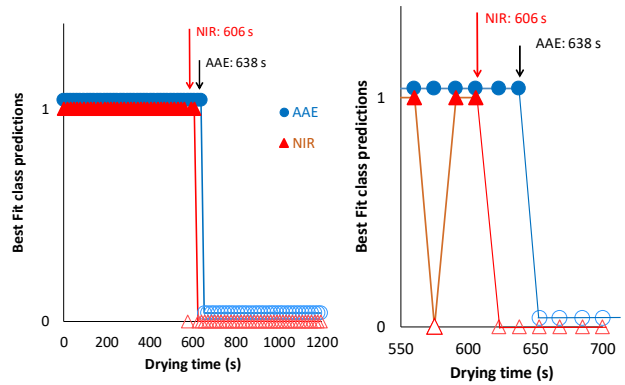

Figure 7

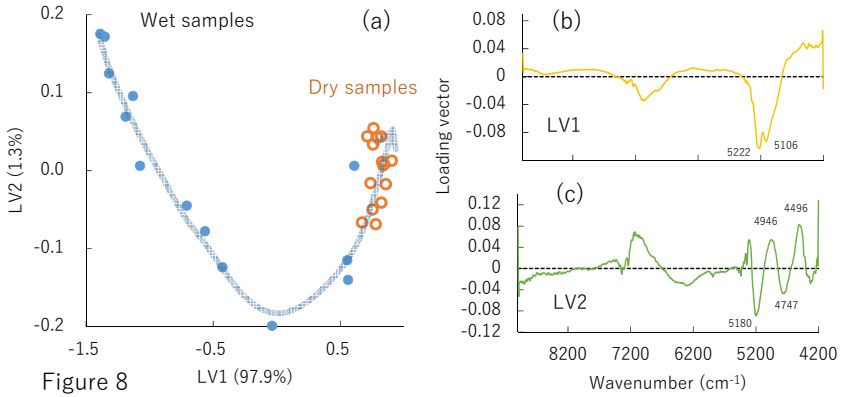

Figure 8

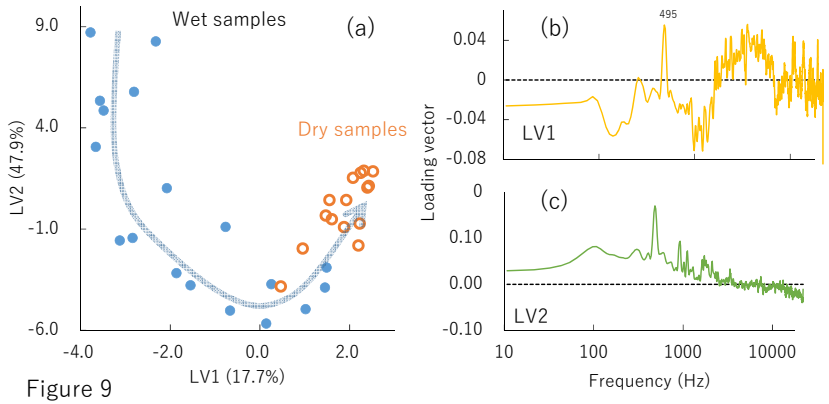

Figure 9

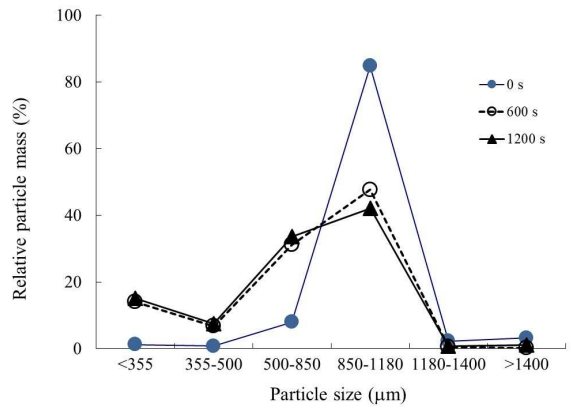

Figure 10

Table 1

	LV	CPV	SECV	PRESS Val	R^2 Val	SEC	PRESS Cal	R^2 Cal
NIR	5	99.9	0.329	3.57	0.999	0.259	1.81	1.000
AAE	5	83.2	1.30	55.9	0.991	0.615	10.2	0.998

Table 2

	LV	CPV	SECV	PRESS Val	R^2 Val	SEC	PRESSCal	R^2 Cal
NIR	5	99.9	0.1842	1.12	0.929	0.136	0.501	0.969
AAE	5	82.2	0.2406	1.91	0.877	0.133	0.476	0.970